PAPER

Check for updates

The impact of metal ions on photoinduced electron-transfer properties: four photochromic metal–organic frameworks based on a naphthalenediimide chromophore†

Hui-Ling Xu,[a] Xiao-Shan Zeng,[a] Jie Li,[a] Yu-Ci Xu,[a]
Hai-Jiang Qiu[a] and Dong-Rong Xiao (iD) *[ab]

Four novel photochromic metal–organic frameworks (MOFs) self-assembled from a naphthalenediimide-based ligand and different metal cations, $[Zn_2(BINDI)(DMA)_2]\cdot 2DMA$ (**1**), $[Cd(H_4BINDI)(H_2BINDI)]\cdot 4DMF$ (**2**), $[Ca_2(HBINDI)Cl(DMA)_3]\cdot DMA$ (**3**), $[Ba_4(BINDI)_2(DMF)_7]\cdot 7DMF$ (**4**) (H_4BINDI = N,N'-bis(5-isophthalic acid)naphthalenediimide), have been synthesized and characterized by single-crystal X-ray diffraction, powder X-ray diffraction, elemental analyses, IR spectroscopy and TG analyses. Compound **1** exhibits a 3D porous framework with an **lvt** topology based on paddle-wheel $Zn_2(COO)_4$ clusters and BINDI as four-connected nodes. Compound **2** features a porous threefold interpenetrating diamondoid framework. Compound **3** shows a microporous 2D double-layer architecture and compound **4** displays a porous two-fold interpenetrated 3D network. Interestingly, these four MOFs exhibit reversible photochromic behaviors with a concomitant eye-detectable color change, but different coloration degrees. The comparison of these MOFs indicates that the electron-withdrawing capabilities of metal cations play a significant role in tuning the photosensitive properties of photochromic MOFs; this result may provide a feasible route for the design and synthesis of photochromic MOFs with controllable photoinduced electron-transfer properties. Moreover, the photomodulated photoluminescence properties of compounds **1–4**, as well as the solvatochromic behaviors of **3** and **4** were also investigated. Additionally, compounds **1–3** are found to be useful as indicators for the qualitative detection of nitrite by naked eye recognition of color change.

Introduction

Metal–organic frameworks (MOFs), which are a class of newly developed porous crystalline materials consisting of metal centers/clusters connected by organic linkers, have evolved to be one of the most fascinating research fields in coordination chemistry and materials chemistry because of their intriguing structural diversity and their wide applications in gas sorption, heterogeneous catalysis, chemical separation, sensing, *etc.*[1–3] In this field, the rational design and synthesis of

photochromic MOFs that can respond to external photo-stimuli is an emerging area of current interest, owing to their potential applications in molecular electronics, fluorescent switches, erasable prints, *etc.*[4–7] For the synthesis of photochromic MOFs, one promising strategy is to introduce photo-active components (such as diarylethene derivatives,[8] viologen derivatives,[9,10] naphthalenediimide (NDI) derivatives,[11,12] and so on[13]) as inherent building blocks of MOFs. Prominent studies based on this strategy have been performed by the groups of Guo, Zhang, Lu, Fu, Banerjee, Han, Lin and others.[8–13] It is conceivable that the introduction of photoactive components into the MOFs may not only incorporate functionality from both inorganic and organic components, but also provide the opportunity to produce novel properties by the synergic interactions between the counterparts.[14] However, because many factors, such as the molecular structure, suitable donors and acceptors, the packing type and orientation between the donor and acceptor moieties, the distance of the pathway for charge transfer, the stability of the charge-separated state, *etc.*,[15a–d] can influence the photochromic properties, and the ions can also influence the photophysical

[a] *College of Chemistry and Chemical Engineering, Southwest University, Chongqing, 400715, PR China. E-mail: xiaodr98@swu.edu.cn; Fax: +86 23 68254000; Tel: +86 23 68252360*
[b] *State Key Laboratory of Structural Chemistry, Fujian Institute of Research on the Structure of Matter, Chinese Academy of Sciences, Fuzhou, Fujian 350002, PR China*

† Electronic supplementary information (ESI) available: Some additional structural figures and tables, PXRD patterns and IR spectra. CCDC numbers 1812090–1812093 for **1–4** contain the supplementary crystallographic data for this paper. For ESI and crystallographic data in CIF or other electronic format see DOI: 10.1039/c8ce00213d

properties,[15e,f] the rational design and synthesis of photochromic MOFs with tunable photosensitivity is still a significant and challenging task, and further research is necessary to enrich and develop this field.

With the above stated aspects in mind, we have attempted to synthesize photochromic MOFs self-assembled from metal cations and ligands containing a photochromic NDI core. NDI derivatives are an attractive class of chemically robust, π-electron-deficient and redox-active molecules, which may undergo a reversible one-electron reduction to form stable radical anions and can thus act as electron acceptors in photoinduced electron transfer (PET) processes.[16] This makes them excellent candidates for the construction of photochromic materials. By using NDI derivatives as ligands, some photochromic MOFs have been synthesized recently.[11,12] However, to the best of our knowledge, no systematic investigation of the relationship between the metal cations and the photosensitivity of NDI-based photochromic MOFs has been reported hitherto. An understanding of the effect of metal cations on the photosensitivity may therefore aid in the rational design of novel photochromic MOFs. For this purpose, comparison of a series of related NDI-based photochromic MOFs containing different metal cations is required. Fortunately, this has been achieved successfully for four microporous photochromic MOFs, namely, $[Zn_2(BINDI)(DMA)_2]\cdot 2DMA$ (1), $[Cd(H_4BINDI)(H_2BINDI)]\cdot 4DMF$ (2), $[Ca_2(HBINDI)Cl(DMA)_3]\cdot DMA$ (3), $[Ba_4(BINDI)_2(DMF)_7]\cdot 7DMF$ (4) ($H_4BINDI = N,N'$-bis(5-isophthalic acid)naphthalenediimide), which exhibit different photosensitive properties due to the different electron-withdrawing capabilities of the metal cations. The crystal structures, photochromism, solvatochromism and photomodulated luminescence properties of these compounds, as well as the modulated effect of metal ions on the photosensitivity, will be represented and discussed in this paper.

Experimental

Materials and general methods

All the chemicals and solvents were commercially purchased and used as received without further purification. Elemental analyses (C, H and N) were performed on a Perkin-Elmer 2400 CHN elemental analyzer. Metal atoms (Zn, Cd, Ca and Ba) were determined using a tps-7000 Plasma-Spec(I) inductively coupled plasma-atomic emission spectrometer (ICP-AES). IR spectra were recorded in the range 400–4000 cm^{-1} on a Bio-Rad FTS-185 FT/IR spectrophotometer using KBr pellets. TG analyses were performed on a NETZSCH STA 449C instrument in flowing N_2 with a heating rate of 10 °C min^{-1}. PXRD data were recorded on a XD-3 diffractometer using Cu Kα radiation. The photochromic reaction was agitated using a continuous wavelength-irradiation xenon lamp (Beijing, 300 W). Electron spin resonance (ESR) measurements were obtained using a Bruker A300 instrument operating in the X-band at room temperature. UV-vis diffuse reflectance spectra were recorded at room temperature on a Varian Cary 500

UV-vis spectrophotometer equipped with an integrating sphere by using $BaSO_4$ as a white standard in the range of 200–800 nm. Excitation and emission spectra were obtained on an F-7000 FL fluorescence spectrophotometer equipped with a 150 W xenon lamp as the excitation source. The point symbol and topological analyses were carried out using the TOPOS program package.[17]

Preparation

Synthesis of $[Zn_2(BINDI)(DMA)_2]\cdot 2DMA$ (1). A mixture of $Zn(NO_3)_2\cdot 6H_2O$ (0.03 g, 0.1 mmol), H_4BINDI (0.03 g, 0.05 mmol) and N,N'-dimethylacetamide (DMA, 3 mL) was stirred for 15 min in air, then transferred and sealed in a 17 mL Teflon-lined autoclave, which was heated at 110 °C for 72 h. After slow cooling to room temperature, light yellow crystals of 1 were filtered off, washed with DMA, and dried at ambient temperature (yield: 63% based on Zn). Elemental analysis (%) calcd for $C_{46}H_{46}N_6O_{16}Zn_2$: C, 51.69; H, 4.31; N, 7.87; Zn, 12.17%. Found: C, 51.56; H, 4.46; N, 7.67; Zn, 12.30%. FT/IR data (cm^{-1}): 3420(br), 1715(m), 1678(m), 1618(s), 1580(w), 1514(w), 1450(w), 1404(m), 1348(s), 1254(m), 1196(w), 1117(w), 1020(w), 986(w), 881(w), 770(w), 744(w), 725(w), 652(w), 598(w), 480(w), 420(w).

Synthesis of $[Cd(H_4BINDI)(H_2BINDI)]\cdot 4DMF$ (2). A mixture of $CdCl_2\cdot 2.5H_2O$ (0.023 g, 0.1 mmol), H_4BINDI (0.03 g, 0.05 mmol), N,N'-dimethylformamide (DMF, 5 mL) and ethanol (1 mL) was stirred for about 15 min in air, then transferred and sealed in a 17 mL Teflon-lined autoclave, which was heated at 80 °C for 72 h. After slow cooling to room temperature, yellowish single crystals of 2 were collected, washed with DMF, and dried at ambient temperature (yield: 31% based on Cd). Elemental analysis (%) calcd for $C_{72}H_{54}CdN_8O_{28}$: C, 54.34; H, 3.39; N, 7.04; Cd, 7.04%. Found: C, 54.21; H, 3.22; N, 6.88; Cd, 7.26%. FT/IR data (cm^{-1}): 3418(br), 2789(w), 2477(w), 1713(m), 1680(s), 1620(w), 1576(m), 1450(w), 1346(s), 1252(w), 1209(m), 1196(w), 1119(w), 1020(w), 984(w), 770(w), 743(w), 687(w), 648(w), 422(w).

Synthesis of $[Ca_2Cl(HBINDI)(DMA)_3]\cdot DMA$ (3). A mixture of $CaCl_2$ (0.022 g, 0.2 mmol) and H_4BINDI (0.06 g, 0.1 mmol) was dissolved in DMA (3 mL). The resulting solution was stirred for 10 min in air and then sealed in a 17 mL Teflon-lined autoclave and heated at 130 °C for 1 day. Orange color crystals were separated after the reaction and washed with DMA and preserved for further application and characterization (yield: 41% based on Ca). Anal. calcd. for $C_{46}H_{47}Ca_2ClN_6O_{16}$ (%): C 52.35, H 4.46, N 7.97 Ca 7.59; found (%): C 52.73, H 4.59, N 7.78 Ca 7.41. FT/IR data (cm^{-1}): 3420(br), 1713(w), 1680(m), 1616(m), 1572(w), 1447(w), 1414(w), 1383(w), 1346(w), 1250(w), 1196(w), 1121(w), 1022(w), 986(w), 770(w), 741(w), 650(w), 422(w).

Synthesis of $[Ba_4(BINDI)_2(DMF)_7]\cdot 7DMF$ (4). A mixture of $Ba(NO_3)_2\cdot 2.5H_2O$ (0.052 g, 0.2 mmol), H_4BINDI (0.06 g, 0.1 mmol) and DMF (3 mL) was stirred for 15 min in air, then transferred and sealed in a 17 mL Teflon-lined autoclave, which was heated at 100 °C for 36 h. After slow cooling to

room temperature, yellowish single crystals of **4** were collected, washed with DMF, and dried at ambient temperature (yield: 31% based on Ba). Elemental analysis (%) calcd for $C_{102}H_{118}Ba_4N_{18}O_{38}$: C, 44.51; H, 4.29; N, 9.16; Ba, 19.93%. Found: C, 44.77; H, 4.38; N, 9.02; Ba, 19.71%. FT/IR data (cm^{-1}): 3414(br), 1715(m), 1680(s), 1620(s), 1572(s), 1441(m), 1410(m), 1369(s), 1346(s), 1248(m), 1194(w), 1119(w), 1047(w), 986(w), 932(w), 912(w), 883(w), 779(w), 770(w), 743(w), 719(w), 650(w), 579(w), 528(w), 424(w).

X-ray crystallography

Suitable single crystals of **1**–**4** were selected for single-crystal X-ray diffraction analysis (diffractometer device type: Super-Nova, Dual, Cu at zero, EosS2). Compounds **1**–**4** were collected with Cu Kα radiation (λ = 1.54184 Å) at 99.98 K, 291.11 K, 291.87 K and 100 K. Absorption corrections were applied using the multiscan technique. Using Olex2,[18] the structures of **1**, **2**, and **4** were solved with the SIR2004 (ref. 19) structure solution program, **3** was solved with the Superflip[20] structure solution program using charge flipping. Moreover, the structures of **1**–**4** were refined with the ShelXL[21] refinement package using least squares minimisation. Non-H atoms were refined with anisotropic temperature parameters. The free solvent molecules are highly disordered in compounds **1**, **2**, and **4**, and attempts to locate and refine the solvent peaks were unsuccessful. The diffused electron densities resulting from these molecules were removed using the SQUEEZE routine of PLATON.[22] Then, the structures were refined again using the data generated. The final formulas of compounds **1**, **2**, and **4** were determined by combining with thermogravimetric analysis (TGA) and elemental analyses. The detailed crystallographic data and structure refinement

parameters for compounds **1**–**4** are summarized in Table 1. Selected bond lengths for **1**–**4** are listed in Table S1.†

Results and discussion

Crystal structure of [Zn₂(BINDI)(DMA)₂]·2DMA (1)

Single-crystal X-ray crystallography analysis reveals that compound **1** crystallizes in the orthorhombic space group *Pbnm* and features an unusual 3D network structure. Its asymmetric unit contains two half Zn(II) ions (Zn1 and Zn2 are half-occupied), one half of a BINDI^{4-} ligand, two half coordinated DMA molecules (O7 and O8 are half-occupied) and one uncoordinated DMA molecule (Fig. S1†). Zn1 and Zn2 exhibit distorted square-pyramidal geometries, in which each Zn(II) is coordinated by four oxygen atoms from four BINDI^{4-} ligands and one oxygen atom from DMA (Zn–O 1.946(4)–2.049(2) Å). The closest two Zn(II) ions are linked by four COO$^-$ groups to form a Zn₂(COO)₄ paddle-wheel secondary building unit (SBU) with a Zn⋯Zn distance of 2.995 Å (Fig. 1a). This SBU is linked by four BINDI^{4-} anions which bridge four adjacent SBUs, extending into a 3D framework structure (Fig. 1c). From the topological point of view, the paddle-wheel Zn₂(COO)₄ motifs and BINDI^{4-} anions can be defined as 4-connected nodes. Thus, the overall structure of **1** can be reduced to a 4-connected **lvt** net with a Schläfli symbol of $(4^2 \cdot 8^4)$ (Fig. 1d). The effective free volume is calculated by PLATON analysis to be 52.5% of the crystal volume (3011.5 Å^3 out of the 5737.6 Å^3 unit cell volume).

Crystal structure of [Cd(H₄BINDI)(H₂BINDI)]·4DMF (2)

Compound **2** crystallizes in a monoclinic system with the space group *I*2/*c*, and the asymmetric unit contains one half of a Cd^{2+} ion, one half of a H₂BINDI^{2-} ligand, and one half of

Table 1 Crystal data and structure refinements for compounds **1**–**4**

Compound	1	2	3	4
Empirical formula	$C_{46}H_{46}N_6O_{16}Zn_2$	$C_{72}H_{54}CdN_8O_{28}$	$C_{46}H_{47}Ca_2ClN_6O_{16}$	$C_{102}H_{118}Ba_4N_{18}O_{38}$
M_r (g mol^{-1})	1065.00	1590.40	1055.50	2750.00
Crystal system	Orthorhombic	Monoclinic	Triclinic	Monoclinic
Space group	*Pbnm*	*I*2/*c*	*P*1̄	*P*2₁/*c*
a (Å)	10.2186(2)	18.5534(2)	9.8893(9)	23.4194(4)
b (Å)	36.8564(9)	22.8539(3)	16.7182(4)	13.9077(2)
c (Å)	15.2343(4)	20.0964(3)	17.3044(4)	33.6040(6)
α (°)	90	90	63.933(2)	90
β (°)	90	107.3541(15)	78.652(7)	90.9341(16)
γ (°)	90	90	86.531(5)	90
V (Å^3)	5737.6(2)	8133.3(2)	2518.6(3)	10 943.8(3)
Z	4	4	2	4
ρ_{calcd} (g cm^{-3})	0.963	1.056	1.392	1.253
μ (mm^{-1})	1.436	2.700	3.491	11.601
F(000)	1668.0	2592.0	1104.0	4004.0
2θ range/°	7.53–147.266	9.22–143.508	9.124–134.158	7.392–145.928
Reflections collected	22 531	37 591	34 834	102 162
Unique data (R_{int})	5894(0.0416)	7885(0.0939)	8945(0.0252)	21 513(0.0580)
GOF on F^2	1.156	1.046	1.096	1.171
$R_1{}^a$/w$R_2{}^b$ [$I > 2\sigma(I)$]	0.0702/0.2199	0.0550/0.1500	0.0699/0.2088	0.0981/0.2966
$R_1{}^a$/w$R_2{}^b$ (all data)	0.0825/0.2314	0.0599/0.1555	0.0779/0.2177	0.1355/0.3198

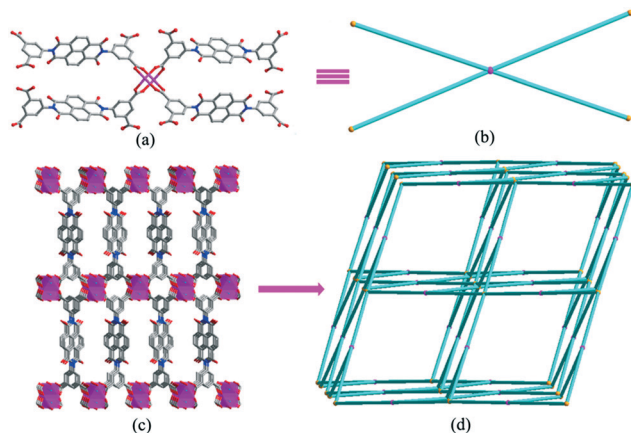^{a} $R_1 = \sum||F_0| - |F_C||/\sum|F_0|$. ^{b} w$R_2 = \sum[w(F_0{}^2 - F_C{}^2)^2]/\sum[w(F_0{}^2)^2]^{1/2}$.

Fig. 1 (a) View of the $Zn_2(COO)_4$ paddle-wheel SBU in **1**. (b) Simplified view of the four-connected $Zn_2(COO)_4$ SBU. (c) Perspective and (d) schematic views of the **lvt** network of **1**.

a H_4BINDI ligand (Fig. S2a†). Each Cd(II) cation is six-coordinated by four carboxylate oxygen atoms from two H_2BINDI^{2-} ligands and two O atoms from two H_4BINDI ligands. The Cd–O bond lengths vary from 2.231(2) to 2.384(2) Å. In the structure of **2**, two carboxyl groups of the H_4BINDI ligand link two Cd(II) cations in a μ_1-η^0:η^1 coordination fashion, whereas the other two carboxyl groups of the H_2BINDI^{2-} anion link two Cd(II) cations in a μ_1-η^1:η^1 mode (modes I and II in Scheme S1†). Based on these connection modes, each Cd atom is linked to four nearest Cd atoms through four linear ligands to generate a 3D framework (Fig. S2b†). The topological analysis of **2** reveals that it is a diamondoid (**dia**) framework. As illustrated in Fig. 2, the single **dia** net is interpenetrated by two identical **dia** nets, giving rise to a 3-fold interpenetrating framework. Notably, even after 3-fold interpenetration, the accessible free volume reached 45.3% of the cell volume, as calculated by PLATON.

Crystal structure of $[Ca_2Cl(HBINDI)(DMA)_3]\cdot DMA$ (3)

Compound **3** crystallizes in the triclinic system with a space group of $P\bar{1}$. Its asymmetric unit comprises two Ca atoms,

one Cl atom, one $HBINDI^{3-}$ ligand, three coordinated DMA molecules and one free DMA molecule (Fig. S3†). Ca1 is six coordinated by five oxygen atoms and one Cl atom. Among the five oxygen atoms, four are from four $HBINDI^{3-}$ ligands and one is from coordinated DMA. Ca2 adopts a seven coordinated mode, which is defined by five carboxylic oxygen atoms from three $HBINDI^{3-}$ ligands and two oxygen atoms from two DMA molecules. Two Ca atoms (Ca1 and Ca2) are joined together by three carboxylate groups, thus forming a binuclear $[Ca_2(COO)_3]$ cluster with a Ca⋯Ca distance of 3.698(2) Å. In **3**, each $HBINDI^{3-}$ links four $[Ca_2(COO)_3]$ clusters to yield a 2D double layer (Fig. 3a). In the packing arrangement of **3**, the adjacent 2D layers are interdigitated with each other to yield a 2D → 3D interdigitated framework (Fig. S4†).

Topologically, both binuclear Ca_2 and $HBINDI^{3-}$ can be simplified as 4-connected nodes. Thus, the 2D layer of **3** can be described as a 4-connected network with a $(4^3 \cdot 6^3)$ topology (Fig. 3b). Moreover, the effective free volume of **3** was calculated by PLATON analysis to be 15.6% of the crystal volume (393.4 Å^3 out of the 2518.6 Å^3 unit cell volume).

Crystal structure of $[Ba_4(BINDI)_2(DMF)_7]\cdot 7DMF$ (4)

X-ray single-crystal structure analysis reveals that **4** crystallizes in the monoclinic space group $P2_1/c$. In the asymmetric unit there are four crystallographically distinct Ba(II) metal centers, two $BINDI^{4-}$ ligands and seven coordinated DMF molecules (Fig. S5†). The four Ba(II) cations exhibit two different coordination geometries. Ba1, Ba2 and Ba4 are nine-coordinated by six carboxylate oxygen atoms from four $BINDI^{4-}$ ligands and three oxygen atoms from three DMF molecules. However, Ba3 is eight-coordinated by six carboxylate oxygen atoms from four $BINDI^{4-}$ ligands and two oxygen atoms from two DMF molecules. The Ba–O bond lengths vary from 2.666(8) to 2.905(11) Å. Each $BINDI^{4-}$ ligand links eight Ba(II) cations with its four carboxylate groups in a μ_2-η^1:η^2 coordination fashion (mode III in Scheme S1†). Two adjacent Ba(II) atoms (Ba1 and Ba2, Ba3 and Ba4) are linked by two carboxylate groups of $BINDI^{4-}$ ligands, forming a rod-shaped $[Ba(\mu_2-O)_2]_n$ chain (Fig. 4a). The distances between two adjacent Ba(II) atoms are 4.201 Å and 4.185 Å. On the basis of this
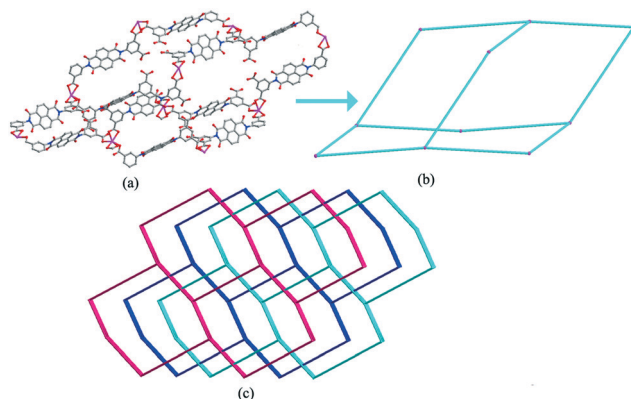

Fig. 2 (a) Perspective and (b) schematic views of the single adamantanoid cage in **2**. (c) Topological representation of the 3-fold interpenetrating **dia** networks in **2**.
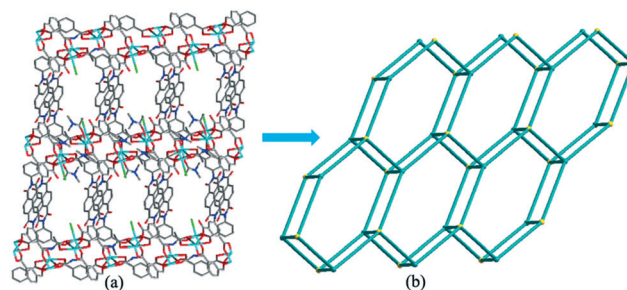

Fig. 3 (a) View of the 2D double layer in **3**. (b) Topological representation of the 2D 4-connected network of the $(4^3 \cdot 6^3)$ topology in **3**.
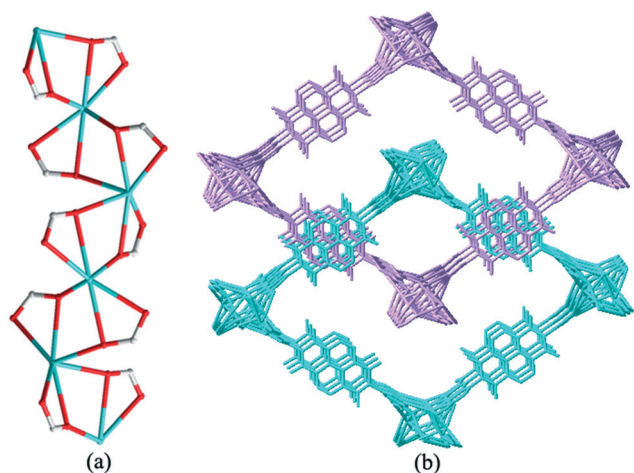
Fig. 4 (a) The infinite rod-shaped SBU in **4**. (b) View of the two-fold interpenetrated 3D framework of **4**.

connection mode, adjacent rod-shaped chains acting as secondary building units (SBUs) are further interconnected by BINDI^{4-} ligands to generate a striking 3D framework with a large channel, as shown in Fig. 4b. The large cavities in the framework lead to the formation of a two-fold interpenetrated porous framework. Although interpenetrated, there is still enough void space in the framework filled with

solvent molecules. After removal of the guest molecules, a total accessible volume of 4239.3 Å^3 per unit cell was determined by using PLATON, which accommodates approximately 38.7% of the unit cell volume (10 943.8 Å^3).

Photochromic properties and qualitative detection of nitrite

The photochromic properties of compounds **1–4** were also examined in air at room temperature. Interestingly, the four MOFs show eye-detectable photochromic transformation upon irradiation using a xenon lamp for 2 minutes. After irradiation, compound **1** exhibited a color change from pale brown-yellow to brownish black, compound **2** changed from light-yellow to dark-brown, compound **3** transformed from yellow into black-green, and compound **4** changed from yellow to dark green (Fig. 5). The irradiated samples of **1–4** can return to the initial color after being held in the dark at room temperature. The time required for reversal to the initial color was found to be 14 days for **1** and **2**, 8 h for **3**, and 2 days for **4**. Their photochromic behaviors have been characterized by UV-vis diffuse-reflectance spectroscopy and electron spin resonance (ESR) measurements (Fig. 5 and 6). As depicted in Fig. 5, the irradiated samples show characteristic bands around 450 nm for **1**, 636 nm for **3** and 627 nm for **4** in the UV-vis diffuse reflectance spectra. The UV-vis spectrum of the as-synthesized crystalline sample of **2**
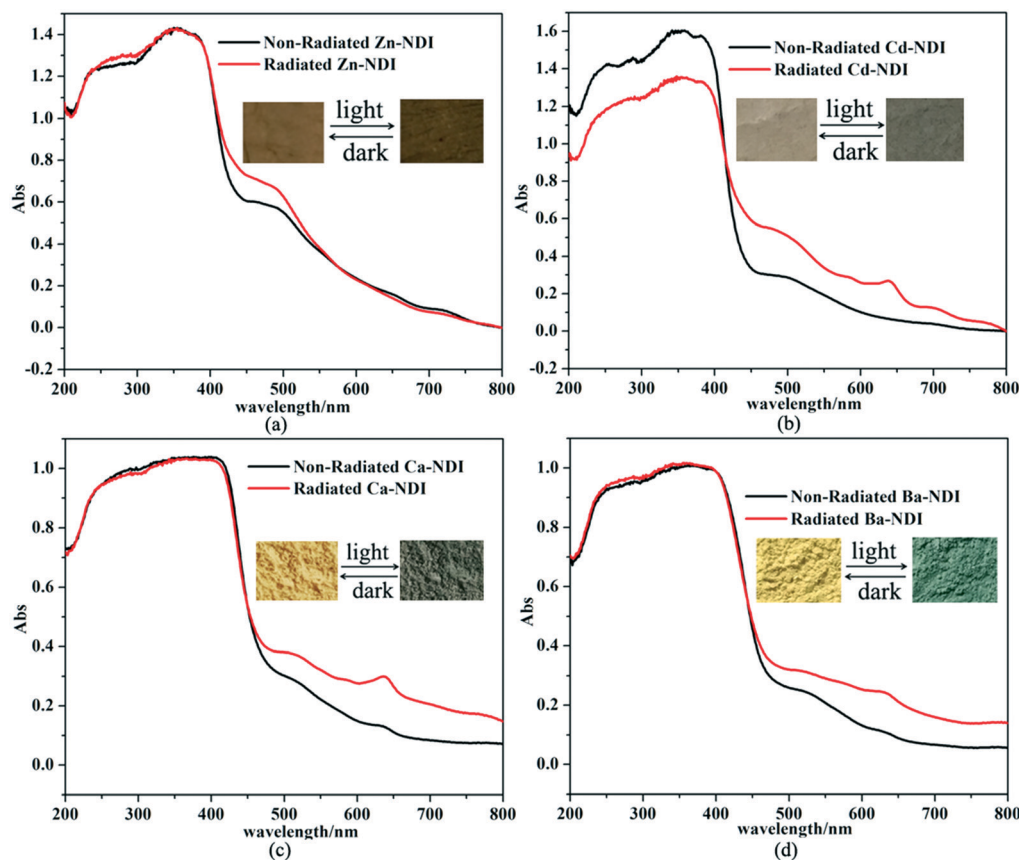

Fig. 5 UV-vis diffuse-reflectance spectra of compounds **1** (a), **2** (b), **3** (c), and **4** (d).
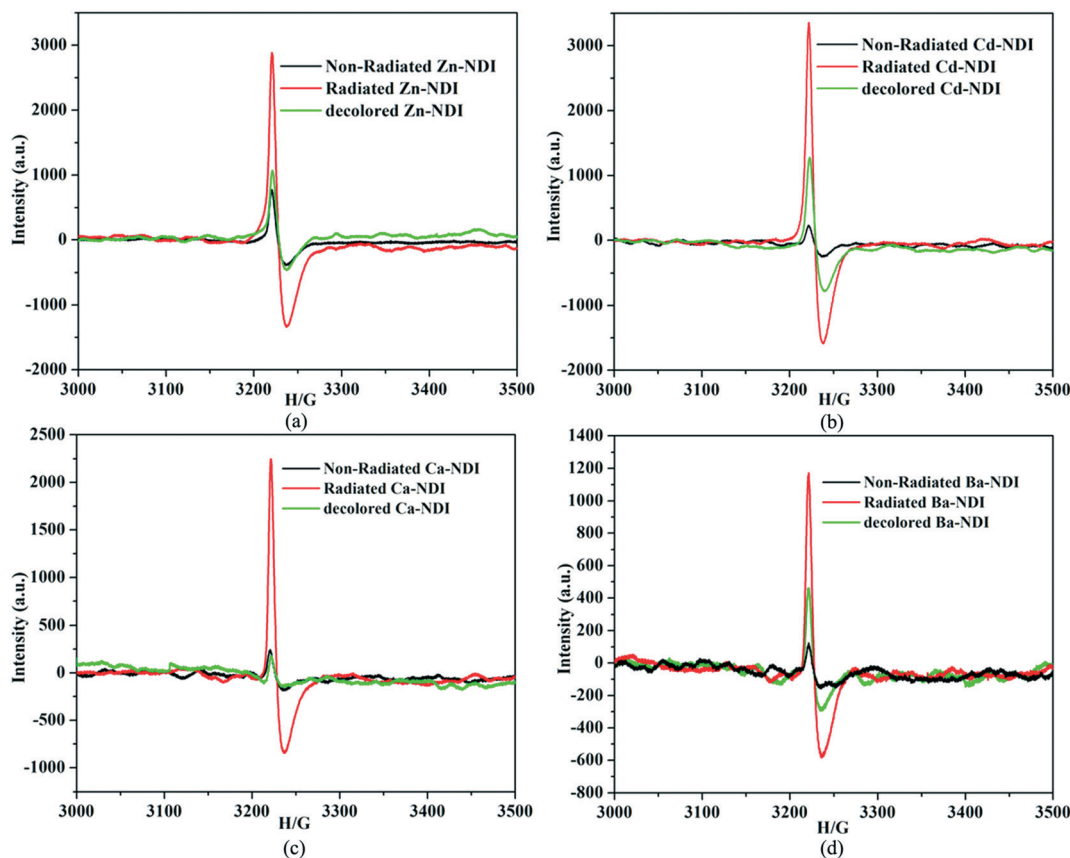
Fig. 6 The ESR spectra of compounds **1** (a), **2** (b), **3** (c), **4** (d) before, after photoirradiation and after decoloration.

exhibits two intense electron absorption bands at 251 and 358 nm. They became weak and a new band at around 636 nm appeared when the sample was illuminated. The results are in agreement with those reported in the literature. The UV-vis spectra of the as-synthesized **1**–**4** show absorption bands in the region 360–380 nm, which are typical for naphthalenediimides. The UV-vis spectra of the irradiated samples **1**–**4** display enhanced absorption in the 450–800 nm region, which may arise from a photo-induced electron-transfer transition.[16e] As we all know, the amount of radicals generated from each compound is closely related to the efficiency of photoinduced electron transfer in the four MOFs. Based on this, semi-quantitative ESR analysis was introduced to compare the amount of photogenerated radicals before and after irradiation under the same conditions. ESR spectroscopy studies of the as-synthesized samples give sharp signals at g = 1.9934 for **1** and **4**, 1.9936 for **2**, and 1.9931 for **3**, and the amount of radicals is in the order of **4** (Ba-NDI) < **3** (Ca-NDI) < **2** (Cd-NDI) < **1** (Zn-NDI) (Fig. S6†), which indicates that compounds **1**–**4** exhibit different photosensitive properties. The larger amount of radicals in the as-synthesized sample of **1** is consistent with its deeper color as compared with others. That is to say, charge separation had already occurred. The generation of NDI radicals for as-synthesized **1**–**4** may be induced by indoor light activation, which is indeed supported by the fact that ESR signals with

enhanced intensity are observed after irradiation (Fig. 6). After decoloration, such radical signals almost returned to the initial state for **1** (Zn-NDI) and **3** (Ca-NDI), but **2** (Cd-NDI) and **4** (Ba-NDI) cannot completely revert to the initial state (Fig. 6). The aforementioned UV-vis and ESR spectral features of the photoproducts resemble those of NDI radical species (NDI˙), which demonstrates that the color change of **1**–**4** arises from the photoinduced ET and the generation of NDI radicals.[11,12]

It is well known that many factors can affect the photochromic properties. In a comparison of these four MOFs, the different coloration degrees exhibited by these four photochromic MOFs demonstrate that metal cations may have a very significant effect on the photosensitivity. The metal cations with stronger electron-withdrawing capabilities are more inclined to get electrons, and thus the corresponding electron deficiency of NDI moieties is higher, which promotes the photoinduced electron transfer reactions. According to the literature,[24] the electronegativity values of cations are in the order of Ba(II) < Ca(II) < Cd(II) < Zn(II). Thus, the electron-withdrawing capabilities of the metal cations are in the order of Ba(II) < Ca(II) < Cd(II) < Zn(II). As a result, the electron deficiency of NDI moieties is in the order of **4** (Ba-NDI) < **3** (Ca-NDI) < **2** (Cd-NDI) < **1** (Zn-NDI). Therefore, the photosensitivity is also in the order of **4** (Ba-NDI) < **3** (Ca-NDI) < **2** (Cd-NDI) < **1** (Zn-NDI). It is worth noting that the photochromic

transformation of **2** and **4** is not easily reversible. The reason may be attributed to the dense packing mode, the 3D 3-fold interpenetrating framework for **2** and the 3D 2-fold interpenetrating network for **4**, which protect the photo-generated NDI radicals from air oxidation. However, the detailed reason needs further elucidation in the future.

Considering that the NDI radical is oxidation sensitive, we have investigated the ability of compounds **1**–**3** to sense nitrite. After addition of sodium nitrite solution (0.1 mmol L^{-1}), the colored samples of **1**–**3** can be bleached to the initial color (Fig. S7–S9†). In particular, such coloration and decoloration processes could be reproduced for a significant number of cycles. The above results indicate that compounds **1**–**3** can be potentially used as indicators for the qualitative detection of trace nitrite in out-of-date foods by naked eye recognition of color change. We also tested the fluorescence responses of the irradiated samples **1**–**3** to the addition of sodium nitrite. Upon irradiation, the fluorescence emission intensities of **1**–**3** decrease. After addition of sodium nitrite solution, their luminescence can be restored accompanying the colour recovery (Fig. S10†).

Photomodulated photoluminescence properties

Considering the photochromism of compounds **1**–**4**, we tested the photocontrolled luminescence of **1**–**4**. The main emission peaks occur at 585 nm for **1** and **2**, 499 nm for **3** and 467 nm for **4** when excited at 280 nm (Fig. 7), and the fluorescence emission intensities of **1**–**4** exhibit a gradual decrease with the increase of irradiation time. Interestingly, their luminescence can be restored accompanying the colour recovery when the samples are left to stand in the dark (Fig. S11†). As shown in Fig. 8, the UV-vis spectra of the irradiated samples **3** and **4** reveal the appearance of an entirely new sharp band with an absorption maximum at 636 nm for **3** and 627 nm for **4**, whose intensity increases with the prolongation of irradiation time. Solid state light reversion of **3** and **4** monitored at 636 nm and 627 nm exhibit approximately first order kinetics (Fig. S12†).

Solvatochromic properties

It should be noted that **3** and **4** show solvatochromic behaviors in the presence of different solvents. When powders **3** and **4** were soaked in DMF, DMA, DEF, MeCN and EtOH, the resulting inclusion compounds undergo an eye-detectable color change (Fig. 9a and 10a). This color change is reversible, as shown in Fig. S13.† Furthermore, the solvent-containing samples maintain their crystallinity, as evidenced by PXRD (Fig. S16†). As depicted in Fig. S14,† the UV-vis absorption bands of solvent@**3** and solvent@**4** exhibit band broadening in the region 475–680 nm, which is dependent
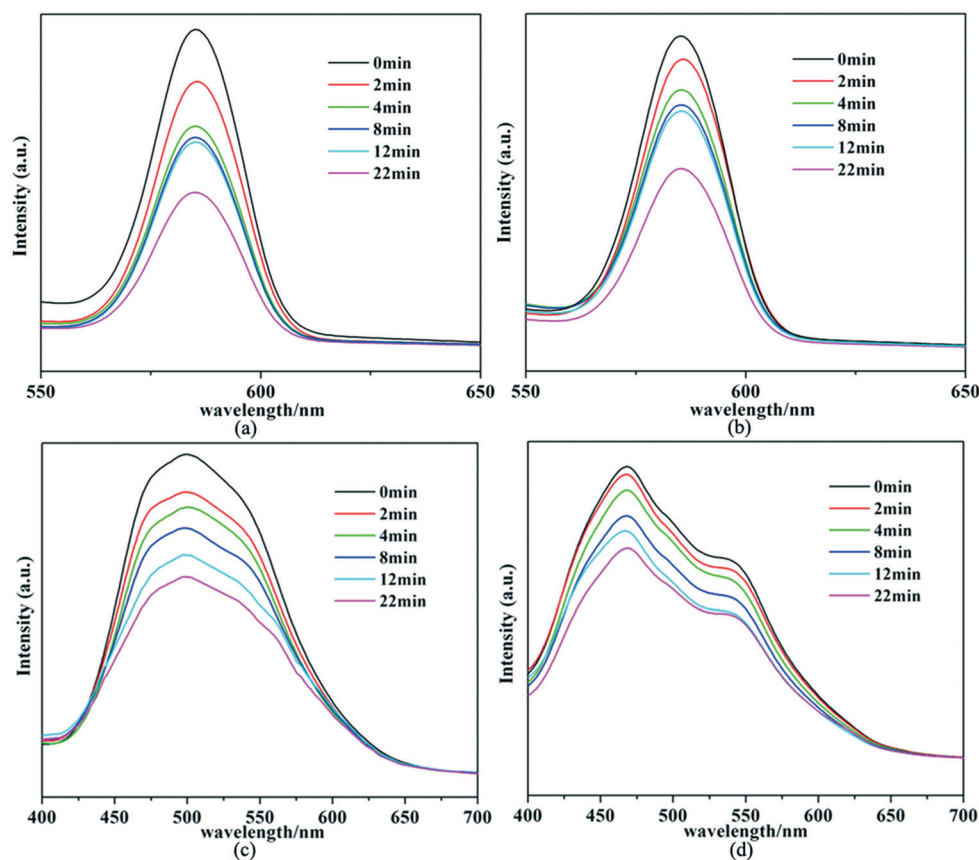

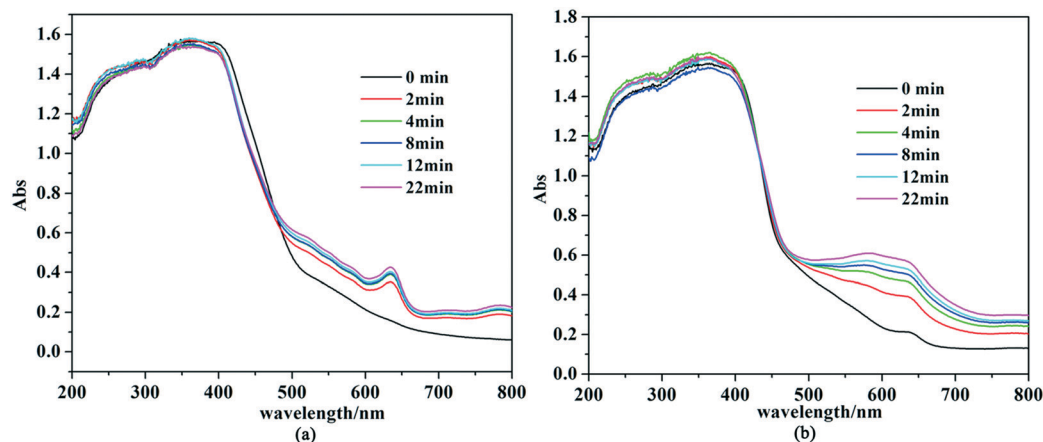**Fig. 7** Fluorescent spectral changes of **1** (a), **2** (b), **3** (c), and **4** (d).

Fig. 8 The UV-vis diffuse reflectance spectral changes of **3** (a), **4** (b) upon light irradiation.
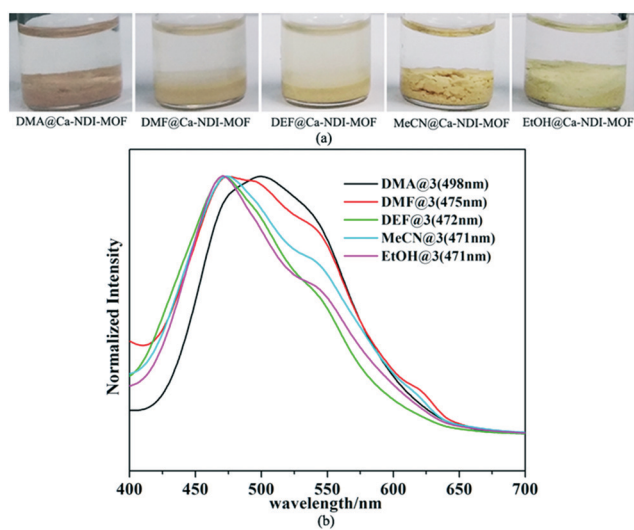

Fig. 9 (a) Visual response of **3** in various solvents. (b) Solid state photoluminescence of **3** soaked in different solvents.
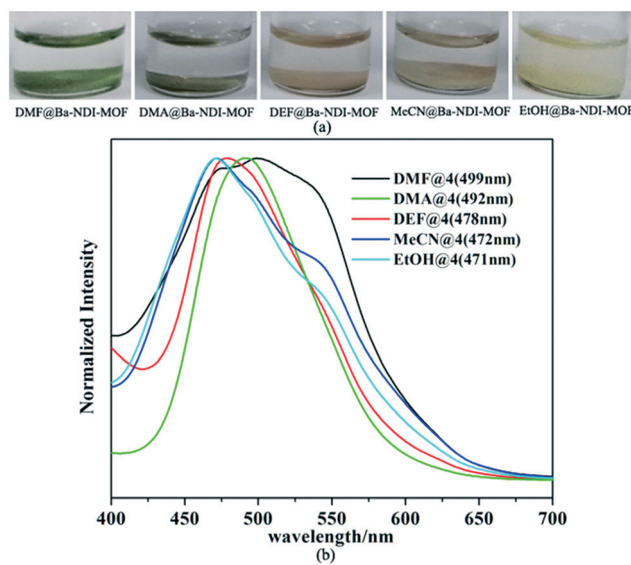

Fig. 10 (a) Visual response of **4** in various solvents. (b) Solid state photoluminescence of **4** soaked in different solvents.

on the polarity of the included solvent. The solvent-dependent photoluminescence of these inclusion compounds is shown in Fig. 9b and 10b. It can be seen that fluorescent emissions occur at 471 nm for EtOH@**3**, 471 nm for MeCN@**3**, 472 nm for DEF@**3**, 475 nm for DMF@**3**, 498 nm for DMA@**3**, 471 nm for EtOH@**4**, 472 nm for MeCN@**4**, 478 nm for DEF@**4**, 492 nm for DMA@**3**, and 499 nm for DMF@**4** (λ_{ex} = 280 nm, Fig. 9b and 10b). The maximum emission peaks of **3** and **4** are shifted hypsochromically, showing a negative solvatochromic effect with increasing polarity of solvent molecules [DMF < DEF < MeCN < EtOH], which may be attributed to the bonding effects between the host and guest.[23]

Conclusions

In summary, we have prepared and characterized four microporous photochromic MOFs assembled from a NDI-related tetracarboxylate ligand and different metal ions. These four MOFs exhibit reversible photochromic and photomodulated luminescence properties. Furthermore, compounds **3** and **4** exhibit solvatochromic properties in the presence of different solvents, and compounds **1**–**3** may find potential application as indicators for the qualitative detection of trace nitrite by a visual color change. More interestingly, due to the different electron-withdrawing capabilities of the metal cations, compounds **1**–**4** exhibit different photosensitive properties. The progressive decrease in the photosensitive properties observed for these four MOFs with a decrease in the electron-withdrawing capabilities of the metal cations shows that the metal cations play an important role in tuning the photosensitivity of photochromic MOFs. It is believed that the preliminary result may provide a promising route for the rational design of photochromic MOFs with tunable photosensitive properties.

Conflicts of interest

There are no conflicts of interest to declare.

Acknowledgements

References

1 (*a*) L. F. Ding and A. O. Yazaydin, *Microporous Mesoporous Mater.*, 2013, **182**, 185; (*b*) P. Falcaro, R. Ricco, C. M. Doherty, K. Liang, A. J. Hill and M. J. Styles, *Chem. Soc. Rev.*, 2014, **43**, 5513; (*c*) K. Gedrich, I. Senkovska, N. Klein, U. Stoeck, A. Henschel, M. R. Lohe, I. A. Baburin, U. Mueller and S. Kaskel, *Angew. Chem., Int. Ed.*, 2010, **49**, 8489; (*d*) J. A. Perman, M. Chen, A. A. Mikhail, Z. Niu and S. Ma, *CrystEngComm*, 2017, **19**, 4171; (*e*) X. Li, Z. H. Li, L. Lu, L. M. Huang, L. Xiang, J. Shen, S. Y. Liu and D. R. Xiao, *Chem. – Eur. J.*, 2017, **23**, 10638.

2 (*a*) J. Lee, O. K. Farha, J. Roberts, K. A. Scheidt, S. T. Nguyen and J. T. Hupp, *Chem. Soc. Rev.*, 2009, **38**, 1450; (*b*) H.-Y. Li, L.-H. Cao, Y.-L. Wei, H. Xu and S.-Q. Zang, *CrystEngComm*, 2015, **17**, 6297; (*c*) J.-R. Li, J. Sculley and H.-C. Zhou, *Chem. Rev.*, 2012, **112**, 869; (*d*) W. Lu, Z. Wei, Z.-Y. Gu, T.-F. Liu, J. Park, J. Park, J. Tian, M. Zhang, Q. Zhang, T. Gentle Iii, M. Bosch and H.-C. Zhou, *Chem. Soc. Rev.*, 2014, **43**, 5561; (*e*) Y.-C. Xu, Y. Chen, H.-J. Qiu, X.-S. Zeng, H.-L. Xu, J. Li, Y.-F. Zeng and D.-R. Xiao, *CrystEngComm*, 2016, **18**, 8182; (*f*) S. Mendiratta, C. H. Lee, M. Usman and K. L. Lu, *Sci. Technol. Adv. Mater.*, 2015, **16**, 054204.

3 (*a*) I. Nath, J. Chakraborty and F. Verpoort, *Chem. Soc. Rev.*, 2016, **45**, 4127; (*b*) J. Rocha, L. D. Carlos, F. A. A. Paz and D. Ananias, *Chem. Soc. Rev.*, 2011, **40**, 926; (*c*) M. Yoon, R. Srirambalaji and K. Kim, *Chem. Rev.*, 2012, **112**, 1196; (*d*) Q. C. Zhang, Y. Liu, X. H. Bu, T. Wu and P. Y. Feng, *Angew. Chem., Int. Ed.*, 2008, **47**, 113; (*e*) L. Chen, J. W. Ye, H. P. Wang, M. Pan, S. Y. Yin, Z. W. Wei, L. Y. Zhang, K. Wu, Y. N. Fan and C. Y. Su, *Nat. Commun.*, 2017, **8**, 15985; (*f*) M. Pan, B. B. Du, Y. X. Zhu, M. Q. Yue, Z. W. Wei and C. Y. Su, *Chem. – Eur. J.*, 2016, **22**, 2440; (*g*) M. Pan, Y. X. Zhu, K. Wu, L. Chen, Y. J. Hou, S. Y. Yin, H. P. Wang, Y. N. Fan and C. Y. Su, *Angew. Chem., Int. Ed.*, 2017, **56**, 14582.

4 (*a*) C.-W. Kung, T. C. Wang, J. E. Mondloch, D. Fairen-Jimenez, D. M. Gardner, W. Bury, J. M. Klingsporn, J. C. Barnes, R. Van Duyne, J. F. Stoddart, M. R. Wasielewski, O. K. Farha and J. T. Hupp, *Chem. Mater.*, 2013, **25**, 5012; (*b*)

5 (*a*) Y. Hasegawa, T. Nakagawa and T. Kawai, *Coord. Chem. Rev.*, 2010, **254**, 2643; (*b*) H.-Y. Li, Y.-L. Wei, X.-Y. Dong, S.-Q. Zang and T. C. W. Mak, *Chem. Mater.*, 2015, **27**, 1327.

6 (*a*) B. Garai, A. Mallick and R. Banerjee, *Chem. Sci.*, 2016, **7**, 2195; (*b*) W.-Q. Kan, S.-Z. Wen, Y.-C. He and C.-Y. Xu, *Inorg. Chem.*, 2017, **56**, 14926.

7 (*a*) L. Han, L.-P. Xu, L. Qin, W.-N. Zhao, X.-Z. Yan and L. Yu, *Cryst. Growth Des.*, 2013, **13**, 4260; (*b*) C. L. Jones, A. J. Tansell and T. L. Easun, *J. Mater. Chem. A*, 2016, **4**, 6714; (*c*) J. Park, D. W. Feng, S. Yuan and H. C. Zhou, *Angew. Chem., Int. Ed.*, 2015, **54**, 430; (*d*) J.-K. Sun and J. Zhang, *Dalton Trans.*, 2015, **44**, 19041; (*e*) R. Pardo, M. Zayat and D. Levy, *Chem. Soc. Rev.*, 2011, **40**, 672.

8 (*a*) B. J. Furlong and M. J. Katz, *J. Am. Chem. Soc.*, 2017, **139**, 13280; (*b*) F. Luo, C. B. Fan, M. B. Luo, X. L. Wu, Y. Zhu, S. Z. Pu, W. Y. Xu and G. C. Guo, *Angew. Chem., Int. Ed.*, 2014, **53**, 9298.

9 (*a*) H. Chen, G. Zheng, M. Li, Y. Wang, Y. Song, C. Han, J. Dai and Z. Fu, *Chem. Commun.*, 2014, **50**, 13544; (*b*) Y.-N. Gong and T.-B. Lu, *Chem. Commun.*, 2013, **49**, 7711; (*c*) J.-K. Sun, L.-X. Cai, Y.-J. Chen, Z.-H. Li and J. Zhang, *Chem. Commun.*, 2011, **47**, 6870; (*d*) J.-K. Sun, P. Wang, Q.-X. Yao, Y.-J. Chen, Z.-H. Li, Y.-F. Zhang, L.-M. Wu and J. Zhang, *J. Mater. Chem.*, 2012, **22**, 12212.

10 (*a*) Y. Tan, Z. Fu, Y. Zeng, H. Chen, S. Liao, J. Zhang and J. Dai, *J. Mater. Chem.*, 2012, **22**, 17452; (*b*) Y. Xiao, S.-H. Wang, Y.-P. Zhao, F.-K. Zheng and G.-C. Guo, *CrystEngComm*, 2016, **18**, 2524.

11 (*a*) L. Han, L. Qin, L. P. Xu, Y. Zhou, J. L. Sun and X. D. Zou, *Chem. Commun.*, 2013, **49**, 406; (*b*) A. Mallick, B. Garai, M. A. Addicoat, P. S. Petkov, T. Heine and R. Banerjee, *Chem. Sci.*, 2015, **6**, 1420; (*c*) Y.-X. Xie, W.-N. Zhao, G.-C. Li, P.-F. Liu and L. Han, *Inorg. Chem.*, 2016, **55**, 549; (*d*) H.-L. Zhang, J.-Z. Liao, W. Yang, X.-Y. Wu and C.-Z. Lu, *Dalton Trans.*, 2017, **46**, 4898; (*e*) X. Fang, X. Yuan, Y.-B. Song, J.-D. Wang and M.-J. Lin, *CrystEngComm*, 2014, **16**, 9090; (*f*) J.-J. Liu, Y.-B. Shan, C.-R. Fan, M.-J. Lin, C.-C. Huang and W.-X. Dai, *Inorg. Chem.*, 2016, **55**, 3680.

12 (*a*) J.-J. Liu, Y. Chen, M.-J. Lin, C.-C. Huang and W.-X. Dai, *Dalton Trans.*, 2016, **45**, 6339; (*b*) J.-J. Liu, Y.-F. Guan, Y. Chen, M.-J. Lin, C.-C. Huang and W.-X. Dai, *Dalton Trans.*, 2015, **44**, 17312; (*c*) J.-J. Liu, Y.-J. Hong, Y.-F. Guan, M.-J. Lin, C.-C. Huang and W.-X. Dai, *Dalton Trans.*, 2015, **44**, 653; (*d*) J.-J. Liu, Y. Wang, Y.-J. Hong, M.-J. Lin, C.-C. Huang and W.-X. Dai, *Dalton Trans.*, 2014, **43**, 17908; (*e*) J.-J. Liu, Y. Wang, M.-J. Lin, C.-C. Huang and W.-X. Dai, *Dalton Trans.*, 2015, **44**, 484.

13 X. Zhang, M.-S. Wang, C. Sun, C. Yang, P.-X. Li and G.-C. Guo, *Chem. Commun.*, 2016, **52**, 7947.

14 (*a*) K. Fu, C. X. Ren, C. Chen, L. X. Cai, B. Tan and J. Zhang, *CrystEngComm*, 2014, **16**, 5134; (*b*) X. H. Jin, J. K. Sun, X. M. Xu, Z. H. Li and J. Zhang, *Chem. Commun.*, 2010, **46**, 4695; (*c*) C. Sanchez, B. Julian, P. Belleville and M. Popall, *J. Mater. Chem.*, 2005, **15**, 3559.

C. R. Wade, M. Y. Li and M. Dinca, *Angew. Chem., Int. Ed.*, 2013, **52**, 13377.

15 (*a*) M. Alvaro, B. Ferrer, V. Fornes and H. Garcia, *Chem. Commun.*, 2001, 2546, DOI: 10.1039/B108964C; (*b*) J.-Z. Liao, J.-F. Chang, L. Meng, H.-L. Zhang, S.-S. Wang and C.-Z. Lu, *Chem. Commun.*, 2017, **53**, 9701; (*c*) Y. S. Park, S. Y. Um and K. B. Yoon, *J. Am. Chem. Soc.*, 1999, **121**, 3193; (*d*) J.-J. Shen, F. Wang, T.-L. Yu, F.-Q. Zhang, L. Tian and Y.-L. Fu, *Dalton Trans.*, 2017, **46**, 5414; (*e*) Y. Li, Y. Zhao, R. Jiang, H. Liu and Y. Li, *Inorg. Chem. Front.*, 2014, **1**, 661; (*f*) Y. W. Yu, Y. J. Li, S. H. Chen, T. F. Liu, Z. H. Qin, H. B. Liu and Y. L. Li, *Eur. J. Org. Chem.*, 2012, **23**, 4287.

16 (*a*) C. F. Leong, B. Chan, T. B. Faust and D. M. D'Alessandro, *Chem. Sci.*, 2014, **5**, 4724; (*b*) M. Pan, X. M. Lin, G. B. Li and C. Y. Su, *Coord. Chem. Rev.*, 2011, **255**, 1921; (*c*) N. Sikdar, K. Jayaramulu, V. Kiran, K. V. Rao, S. Sampath, S. J. George and T. K. Maji, *Chem. – Eur. J.*, 2015, **21**, 11701; (*d*) S. L. Suraru and F. Wurthner, *Angew. Chem., Int. Ed.*, 2014, **53**, 7428; (*e*) M. Pan, X. M. Lin, G. B. Li and C. Y. Su, *Coord. Chem. Rev.*, 2011, **255**, 1921; (*f*) L. J. McCormick and D. R. Turner, *CrystEngComm*, 2013, **15**, 8234.

17 V. A. Blatov, *Struct. Chem.*, 2012, **23**, 955.

18 O. V. Dolomanov, L. J. Bourhis, R. J. Gildea, J. A. K. Howard and H. Puschmann, *J. Appl. Crystallogr.*, 2009, **42**, 339.

19 M. C. Burla, R. Caliandro, M. Camalli, B. Carrozzini, G. L. Cascarano, L. De Caro, C. Giacovazzo, G. Polidori, D. Siliqi and R. Spagna, *J. Appl. Crystallogr.*, 2007, **40**, 609.

20 L. Palatinus, S. J. Prathapa and S. van Smaalen, *J. Appl. Crystallogr.*, 2012, **45**, 575.

21 G. M. Sheldrick, *Acta Crystallogr., Sect. A: Found. Crystallogr.*, 2008, **64**, 112.

22 A. L. Spek, *J. Appl. Crystallogr.*, 2003, **36**, 7.

23 J. S. Ovens and D. B. Leznoff, *Chem. Mater.*, 2015, **27**, 1465.

24 K. Li and D. Xue, *J. Phys. Chem. A*, 2006, **110**, 11332.